Amino Acids (2012) 42:2343–2351
DOI 10.1007/s00726-011-0976-1

ORIGINAL ARTICLE

Imaging tumor-induced sentinel lymph node lymphangiogenesis with LyP-1 peptide

Fan Zhang · Gang Niu · Xin Lin · Orit Jacobson · Ying Ma · Henry S. Eden · Yulong He · Guangming Lu · Xiaoyuan Chen

Received: 17 April 2011 / Accepted: 4 July 2011 / Published online: 19 July 2011

Abstract Lymphangiogenesis in tumor-draining lymph nodes (LNs) starts before the onset of metastasis and is associated with metastasis to distant LNs and organs. In this study, we aimed to visualize tumor-induced lymphangiogenesis with a tumor lymphatics-specific peptide LyP-1. The LyP-1 peptide was labeled with a near-infrared fluorophore (Cy5.5) for optical imaging. At days 3, 7, 14 and 21 after subcutaneous 4T1 tumor inoculation, Cy5.5-LyP-1 was administered through the middle phalanges of the upper extremities of the tumor-bearing mice. At 45 min and 24 h postinjection, brachial LN fluorescence imaging was performed. Ex vivo fluorescence images were acquired for quantitative analysis of the fluorescence intensity. Tumor-induced lymphangiogenesis was confirmed by LYVE-1 immunostaining and increased size of tumor side brachial LNs. Cy5.5-LyP-1 staining in LNs co-localized with LYVE-1, suggesting lymphatics-specific binding of LyP-1 peptide. The brachial LNs were clearly visualized by optical imaging at both time points. The tumor side LNs showed significantly higher fluorescence intensities than the contralateral brachial LNs at days 7, 14, and 21, but not day 3 after tumor inoculation. At day 21 after tumor inoculation, the average signal of tumor-draining LNs was 78.0 ± 2.44, 24.3 ± 5.43, 25.6 ± 0.25 ($\times 10^3$ photon/cm^2/s) using Cy5.5-LyP-1, Cy5.5-LyP-1 with blocking, and Cy5.5 only, respectively. Tumor-draining brachial LNs showed extensive growth of lymphatic sinuses throughout the cortex and medulla. Use of LyP-1 based imaging probes with optical imaging offers a useful tool for the study of tumor-induced lymphangiogenesis. LyP-1 may serve as a marker of lymphangiogenesis useful in detecting "high risk" LNs before tumor metastasis and after micro-metastasis, as well as for screening potential anti-lymphatic therapies.

Keywords Lymphangiogenesis · Lymph node · LyP-1 peptide · Optical imaging

F. Zhang and G. Niu contributed equally to this work.

F. Zhang · Y. He · G. Lu (✉)
Department of Radiology, Nanjing Jinling Hospital, Clinical School of the Medical College of Nanjing University, Nanjing 210002, China
e-mail: cjr.luguangming@vip.163.com

F. Zhang · G. Niu · X. Lin · O. Jacobson · Y. Ma · X. Chen (✉)
Laboratory of Molecular Imaging and Nanomedicine (LOMIN), National Institute of Biomedical Imaging and Bioengineering (NIBIB), National Institutes of Health (NIH), Bethesda, MD 20892, USA
e-mail: shawn.chen@nih.gov

G. Niu
Imaging Sciences Training Program, Radiology and Imaging Sciences, Clinical Center and National Institute Biomedical Imaging and Bioengineering, NIH, Bethesda 20892, USA

H. S. Eden
Intramural Research Program, National Institute of Biomedical Imaging and Bioengineering, National Institutes of Health, Bethesda, MD 20892, USA

Introduction

Regional lymph node (LNs) metastasis represents the first step of tumor dissemination for a variety of common human cancers, such as carcinomas of the breast, colon, and prostate as well as melanoma (Tammela and Alitalo 2010). One mechanism that promotes metastasis to regional LNs is tumor-induced LN lymphangiogenesis, which usually precedes metastasis and leads to increased tumor spread to distal LNs and further to distal organs

(Harrell et al. 2007; Ji 2009). It has been found that tumor-associated lymphangiogenesis correlates with metastasis to tumor-draining LNs in several mouse models (Mandriota et al. 2001; Stacker et al. 2001). The lymphangiogenesis of LNs has been shown to be associated with the presence of non-sentinel LN metastases in animal tumor models (Harrell et al. 2007; Hirakawa et al. 2005, 2007; Qian et al. 2006) and human breast cancer and melanoma (Van den Eynden et al. 2007). The induction of sentinel LN lymphangiogenesis may be driven by VEGF-A and VEGF-C in transgenic mouse models (Hirakawa et al. 2005, 2007), which suggests that tumor-secreted factors are also strong mediators for local LN lymphangiogenesis (Ji 2009) and that increased sentinel LN lymphangiogenesis is involved in lymphatic spread of tumor cells (Ishii et al. 2010). In mouse models of skin carcinogenesis in which VEGF-A or VEGF-C was overexpressed in the skin, lymphangiogenesis was found to occur not only at the tumor site but also in the tumor-draining LNs, and to correlate with metastasis to LNs and beyond (Hirakawa et al. 2007).

Conventional in vivo imaging approaches for cancer metastases in patients have focused on the detection of the cancer cells themselves (Jaffer and Weissleder 2005; Sharma et al. 2008). These methods have limited sensitivity, because relatively large anatomical sizes are required for reliable detection (Winnard et al. 2008). In addition, current-imaging approaches to evaluate LN metastasis mainly rely on the size and the shape of the involved LN (Qian et al. 2006). However, nodal metastases are often microscopic, so neither computed tomography (CT) nor standard magnetic resonance (MR) imaging can rule them out reliably (Eiber et al. 2010). Thus, the ability to detect LN lymphangiogenesis may serve as a novel way of predicting LN metastasis. Furthermore, imaging lymphangiogenesis in vivo will be of great help in understanding LN lymphangiogenesis, as well as in developing therapeutics to control metastatic tumor cell dissemination through the lymphatics.

Therefore, various groups have performed studies to develop lymphatic imaging probes that would exceed the capabilities of the established "blue dye" procedure, and to improve the identification and mapping of LNs, especially sentinel LNs during surgery (Ballou et al. 2007; Kosaka et al. 2009; Ting et al. 2010). Targeted optical probes for lymphatic imaging have also been developed, using a near-infrared (NIR) fluorescent indotricarbocyanine (Cy7) dye, that are based on monoclonal antibody recognition of endothelial ligands for the lymphocyte homing receptor L-selectin, MECA-79. These new probes have provided specific LN NIR fluorescent signals detectable within minutes after tail vein injection, and stable imaging has persisted for more than 24 h (Licha et al. 2005). Recently, in mouse models of LN lymphangiogenesis, Mumprecht et al. (2010) found that systemically injected antibodies against lymphatic epitopes accumulated in the lymphatic vasculature in tissues and LNs. Using an ^{124}I-labeled antibody against the lymphatic vessel endothelial hyaluronan receptor-1 (LYVE-1), they found that anti-LYVE-1 immuno-PET enabled visualization of lymphatic vessel expansion in LNs bearing metastases, even though the metastases were not detected by ^{18}F-FDG PET.

Compared with antibodies, peptide-based imaging probes with much smaller molecular size would allow faster clearance and lower immunogenicity. With peptidic phage display screening on MDA-MB-435 xenografts, Laakkonen et al. (2002) identified a cyclic 9-amino-acid peptide (CGNKRTRGC), LyP-1. They found that LyP-1 peptide targeted to lymphatic endothelial cells instead of blood vessel endothelial cells, suggesting that this peptide could be used as a tumor lymphatics specific marker. Intravenous injection of fluorescein-conjugated LyP-1 led to good accumulation in primary MDA-MB-435 xenografts and their metastases. In addition, systemic LyP-1 peptide treatment of xenografted tumor mice inhibited tumor growth (Laakkonen et al. 2004). In this study, we explored the feasibility of LyP-1 peptide probes for LN lymphangiogenesis imaging.

Materials and methods

General

Cy5.5-*N*-hydroxysuccinimide ester (Cy5.5-NHS) was purchased from GE Healthcare (Piscataway, NJ, USA). LyP-1 peptide was purchased from C.S. Bio (Menlo Park, CA, USA). All other solvents and chemicals were purchased from Sigma-Aldrich (St. Louis, MO, USA).

Synthesis of Cy5.5-LyP-1 conjugate

LyP-1 peptide (1 mg, 1 μmol) dissolved in 100 μL of DMSO was mixed with Cy5.5-NHS (GE Healthcare, Piscataway, NJ, USA) (1 mg, 0.89 μmol) and diisopropylethylamine (DIEA, 2 μL). The reaction mixture was stirred in darkness at room temperature for 1 h and then quenched by 10 μL of acetic acid. The crude product was purified by reversed-phase high-performance liquid chromatography (RP-HPLC) on a C_{18} Vydac protein and peptide column (218TP510; 5 μm, 250 × 10 mm). The fractions containing Cy5.5-LyP-1 were collected, lyophilized, and dissolved in saline at a final concentration of 1 mg/mL. For analytical HPLC, a C_{18} Vydac 218TP54 column (5 μm, 250 × 4.6 mm) was used and the flow was set at 1 mL/min using a gradient system starting from 95% solvent A (0.1%

trifluoroacetic acid (TFA)] in water) and 5% solvent B (0.1% TFA in acetonitrile (CAN)) (0–2 min) and ramped to 35% solvent A and 65% solvent B at 32 min. The Cy5.5-LyP-1 peptide had a retention time of 16.05 min. The identity of Cy5.5-LyP-1 was confirmed by MALDI-TOF MS (*m/z*: observed 1,890.70 [M + H^+], calculated 1,888.15) (Fig. 1a). For serum stability assay, 0.5 μg of Cy5.5-LyP-1 peptide was added to 100 μL mouse serums and incubated at 37°C for various periods of time up to 24 h and aliquots were taken and quenched by adding 100 μL acetonitrile. Each aliquot was centrifuged at 5,000 rpm for 5 min. The supernatant (10 μL) was analyzed by LC–MS.

Tumor model development

The 4T1 murine breast cancer cell line was derived from a spontaneously arising BALB/c mammary tumor (Aslakson and Miller 1992). The rapid and efficient metastasis to organs affected in human breast cancer makes the 4T1 model an excellent mouse model for the study of metastatic progression of breast cancer in humans. Moreover, the model is syngeneic in immunocompetent BALB/c mice, which can be used to study the role of the immune system in tumor growth and metastasis (Tao et al. 2008). The cell line was obtained from the American Type Culture Collection (ATCC) (Manassas, VA) and maintained at 37°C in a humidified atmosphere containing 5% CO_2 in Dulbecco's Modification of Eagles Medium (DMEM) with 10% fetal bovine serum (FBS). The tumor model was developed in 4–6 week-old female BALB/C mice (Harlan Laboratories) by subcutaneous injection of 5×10^6 of 4T1 cells to the right shoulder of each mouse. Tumor growth was followed by caliper measurements made perpendicular to the tumors. Animal procedures were performed according to a protocol approved by the National Institutes of Health Clinical Center Animal Care and Use Committee (NIH CC/ACUC).

In vivo optical imaging with Cy5.5-LyP-1

At days 3, 7, 14 and 21 after inoculation with 4T1 cells, tumor-bearing BALB/C mice ($n = 5$/group), under

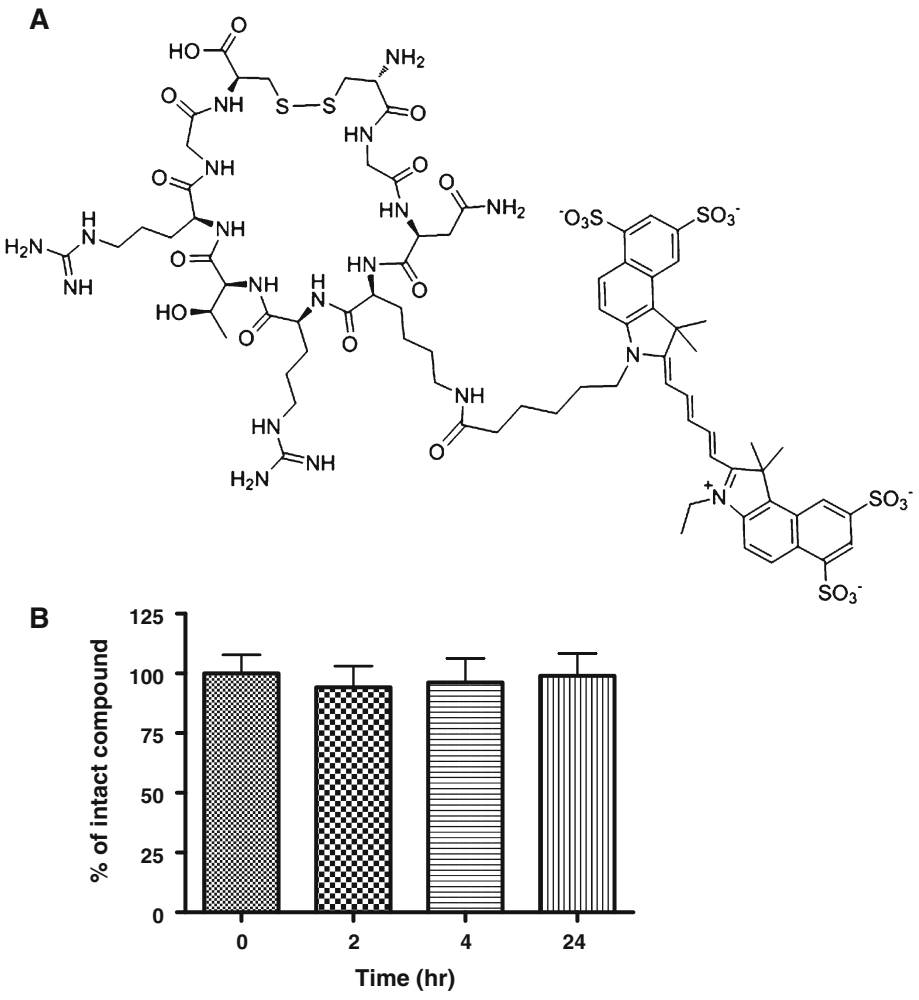

Fig. 1 **a** Structure of Cy5.5-LyP-1. **b** Serum stability of Cy5.5-LyP-1 with LC–MS

isoflurane anesthesia, were injected with either Cy5.5-LyP-1 (0.8 nmol) or Cy5.5 (0.8 nmol) via the middle phalanges of the upper extremities of both sides. At 45 min after injection, in vivo fluorescence imaging was performed with a Maestro II small-animal in vivo imaging system (CRI, Woburn, MA, USA). A filter set with 615–665 nm excitation and long-pass >600 nm emission was used to detect Cy5.5 fluorescent signal. The fluorescence images consisting of Cy5.5 and autofluorescence spectra were then unmixed, based on their spectral patterns, using the manufacturer's software (Maestro software, CRI). At 24 h post injection, the mice were killed and a dorsal skin flap was elevated to expose the brachial LNs on both sides for reimaging of fluorescence. Then the LNs were removed, and ex vivo fluorescence images were obtained to measure the fluorescence intensity. To study the LN specificity of LyP-1 peptide, Cy5.5-LyP-1 was co-injected with 300 μg of un-conjugated LyP-1 peptide as blocking agent.

Histological evaluation and immunofluorescence staining

At 24 h after Cy5.5-LyP-1 injection, brachial LNs from both sides were removed and embedded in optimum cutting temperature (O.C.T.) formulation (Sakura Finetek, Torrance, CA). Then the LNs were sectioned into 4 μm slices and observed with an Olympus IX81 fluorescence microscopy (Olympus Inc., Melville, NY, USA) equipped with an excitation band-pass filter (530–585 nm) and emission band-pass filter (605–680 nm). The same LN sections were also stained against lymphatic endothelial marker LYVE-1. Rabbit anti-mouse LYVE-1 antibody (1:100; Abcam) and FITC-conjugated goat anti-rabbit secondary antibody (1:400; Jackson ImmunoResearch Laboratories) were used. H&E staining was also performed on LN sections.

Measurement and statistical analysis

Fluorescence intensity was measured by drawing regions of interest (ROIs) over removed LNs. Quantitative data were expressed as means ± SD. Means were compared using a Student's t test. $P < 0.05$ was considered statistically significant.

Results

Optical imaging of lymphangiogenesis

Cy5.5-LyP-1 peptide showed high serum stability. Even after 24 h incubation, we did not observe apparent degradation of the peptide as determined by LC–MS (Fig. 1b). Then, we established the tumor model by subcutaneous injection of murine breast cancer 4T1 cells on the right shoulder of BALB/C mice. In this model, the lymph flow drains into the collateral brachial LN, i.e. tumor-draining LN. Compared with the contralateral brachial LN, the tumor-draining brachial LN was significantly enlarged at days 7, 14 and 21 after inoculation (Fig. 2). At 45 min after Cy5.5-LyP-1 injection via the middle phalanges of both upper extremities, brachial LNs on both sides were detectable with in vivo optical imaging. At day 3 after tumor cell inoculation, we did not observe significant fluorescence intensity increase in the tumor-draining LNs over the contralateral brachial LN. From day 7, fluorescence intensity of the tumor-draining brachial LN was progressively elevated. Meanwhile, there was no apparent fluorescent signal change in the contralateral LN (Fig. 3a, b). At the 24 h time point, the primary tumor was removed for optimal LN visualization. The tumor-draining LN still retained a high fluorescent signal after the removal of the primary tumor, especially in mice at 21 days after tumor inoculation. No apparent changes were observed in the contralateral LNs (Fig. 3c, d).

Ex vivo optical imaging of brachial LNs is shown in Fig. 4. Both the size and the fluorescence intensity of the tumor-draining LNs increased along with the time after tumor inoculation from day 7 to 21. The fluorescence intensities were 0.024 ± 0.002, 0.038 ± 0.002, 0.048 ± 0.002 and $0.106 \pm 0.002 \times 10^6$ photon/cm^2/s, respectively, at days 3, 7, 14 and 21 after tumor cell inoculation, which were 1.02, 1.63, 2.04, and 4.52-fold higher than in the contralateral LNs (Fig. 4b).

In order to confirm the specificity of LyP-1 peptide for lymphoangiogenesis imaging, optical imaging with Cy5.5 dye only was performed using the same tumor model as described above. Cy5.5 dye also showed LN uptake and retention at 24 h after local injection (Fig. 5). However, Cy5.5-LyP-1 showed significantly higher LN uptake compared with Cy5.5 ($P < 0.05$ at day 14 and $P < 0.01$ at day 21). More importantly, average signal of Cy5.5-LyP-1 in the LNs also showed significant increase from day 14 to 21 while there was no apparent change with Cy5.5 only along with time. We also performed optical imaging using Cy5.5-LyP-1 with the presence of extra amount of cold LyP-1 peptide. At day 21, the average signal in the LNs after blocking is similar to that of Cy5.5 only, which is significantly lower when compared with unblocked Cy5.5-LyP-1 imaging (Fig. 5).

Histological analysis of tumor induced lymphangiogenesis

To further demonstrate the lymphatic targeting of LyP-1 peptide, the tumor-draining brachial LNs were sectioned

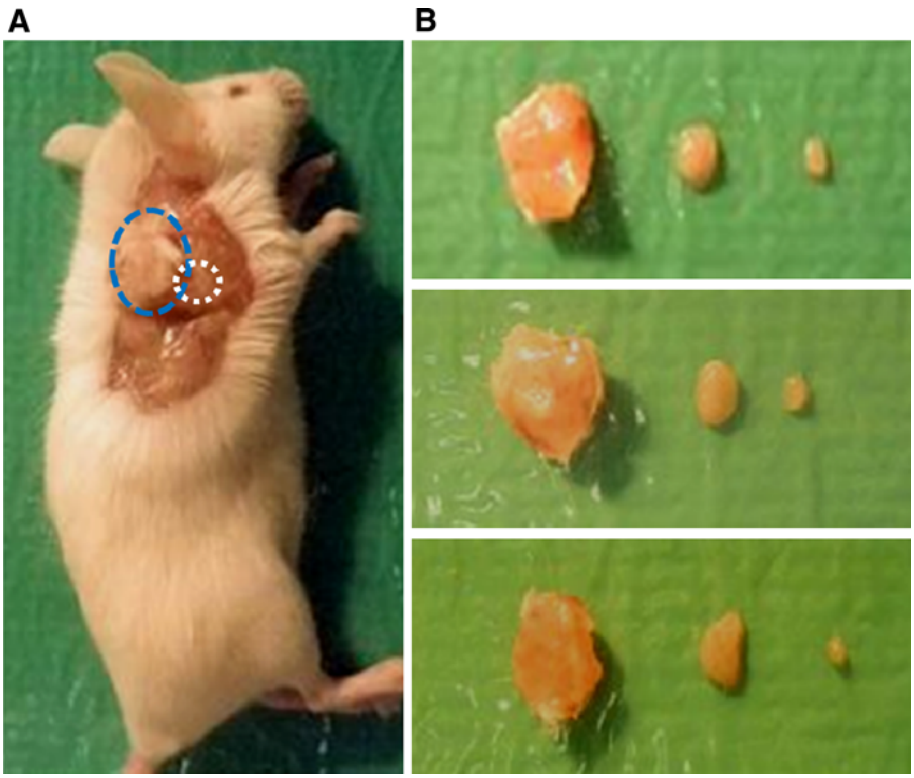

Fig. 2 **a** Relative position of primary tumor (*left circle*) and tumor-draining LN (*right circle*). **b** Photographs of three sets of tumors (*left*), tumor-draining lymph nodes (*middle*) and contralateral lymph nodes (*right*)

after ex vivo fluorescence imaging, and fluorescent signals from Cy5.5-LyP-1 were observed with microscopy. As shown in Fig. 6, Cy5.5-LyP-1 had a vessel-oriented distribution, and the abundance increased along with time after tumor inoculation. Since LYVE-1 is one of the most specific and widely used lymphatic endothelial markers, we stained the LN sections with anti-LYVE-1 antibody and visualized the staining with an FITC-conjugated secondary antibody. At day 3 after tumor inoculation, the tumor-draining LN showed few lymphatic sinuses. At day 7, the tumor-draining LN showed sparse lymphatic sinuses restricted to the cortex. Lymphangiogenesis was consistently observed from day 14 to 21. At day 21, extensive lymphangiogenesis throughout the cortex and medulla was observed.

Interestingly, Cy5.5-LyP-1 showed a distribution pattern in the tumor-draining LNs that was very similar to the staining pattern of anti-LYVE-1 within these same nodes, confirming the lymphatic endothelium's recognition of the LyP-1 peptide. We also noticed that Cy5.5-LyP-1 distribution and anti-LYVE-1 staining did not fully overlap, indicating that LyP-1 does not necessarily bind to LYVE-1.

Discussion

Lymphangiogenesis involves new lymphatic budding, sprouting, and remodeling. Moreover, lymphangiogenesis requires lymphatic endothelial cell (LEC) differentiation to form mature lymphatic networks, and this complicated process is regulated by multiple growth factors, cytokines and chemokines (Ji 2009). Previous studies have demonstrated that lymphangiogenesis in the LNs in the postnatal period is considered to be a major contributor to tumor metastasis (Hirakawa et al. 2009; Ji 2006). Since sentinel LNs are the first destinations in the spreading of cancer in many malignancies, lymphangiogenesis in the sentinel LNs may actively promote lymphatic metastasis. In a B16F10 melanoma model, greatly increased and enlarged lymphatic sinuses were found to be distributed throughout the cortex and medulla in tumor-draining LNs, preceding tumor metastasis (Harrell et al. 2007). Consistent with their findings, we also indentified apparent lymphangiogenesis in tumor-draining LNs in a subcutaneous 4T1 murine breast cancer model. The enlargement of tumor-draining LNs, but not of the contralateral LNs, was observed at day 7 after tumor cell inoculation. LYVE-1 is a hyaluronic acid receptor with sequence similarity to CD44 expressed on LECs (Banerji et al. 1999). Anti-LYVE-1 immunostaining confirmed that extensive lymphangiogenesis happened in the tumor-draining LN. At the early stage of tumor growth, the tumor-draining LNs showed lymphatic sinus expansion mainly in medullary sinuses, and the LN lymphangiogenesis was in the cortical sinuses. Along with time, enlarged lymphatic sinuses and lymphangiogenesis were distributed throughout the cortex and medulla, though we did not

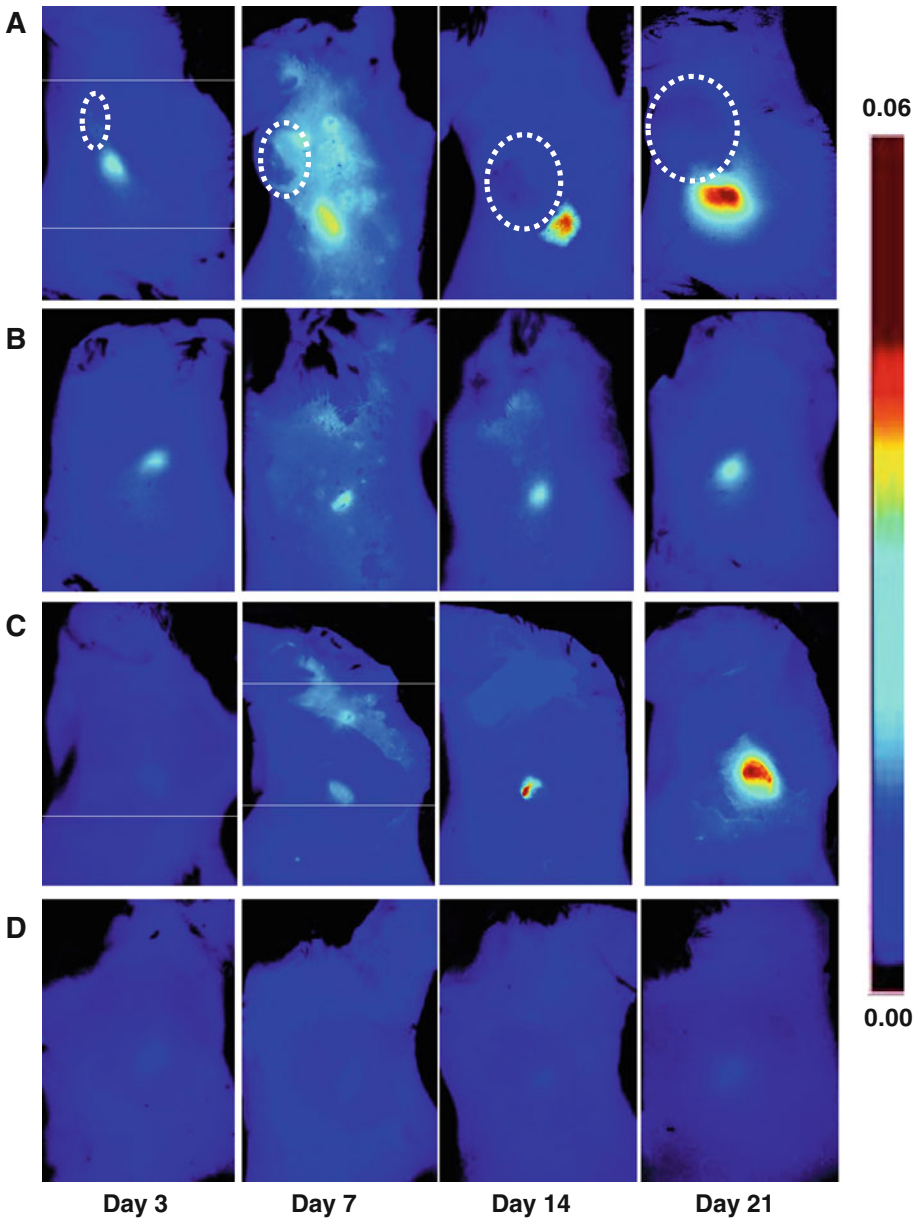

Fig. 3 Optical imaging of tumor-induced lymphangiogenesis with Cy5.5-LyP-1. At days 3, 7, 14 and 21 after 4T1 cell inoculation, tumor-bearing BALB/C mice ($n = 5$/group), under isoflurane anesthesia, were injected with Cy5.5-LyP-1 via the middle phalanges of both upper extremities. At 45 min after injection, in vivo fluorescence imaging of both tumor-draining LNs (**a**) and contralateral LNs (**b**) was performed with a Maestro II small-animal in vivo imaging system. The fluorescence images consisting of Cy5.5 and autofluorescence spectra were then unmixed based on their spectral patterns with the manufacturer's software (Maestro software, CRI). The tumors are indicated by *circles*. (**c**, **d**) At 24 h post injection, the mice were killed and a dorsal skin flap was elevated to expose the brachial lymph nodes on both sides for a repeat of fluorescence imaging (**c** tumor-draining LNs; **d** contralateral LNs)

identify tumor metastases in the tumor-draining LNs by H & E staining at day 21 after tumor inoculation.

In clinical practice, lymphatic mapping employs radiocolloid solutions (Schirrmeister et al. 2004) or vital dyes (Suzuki et al. 2009). These strategies work well to provide information about the localization and function of LNs. However, the signals are transient and only provide non-specific visualization of the lymphatic system. Recent developments in optical imaging in conjunction with various molecular markers offer help in better understanding of the mechanisms underlying lymphangiogenesis and lymphatic metastases of tumors. For example, fluorescently labeled monoclonal anti-mouse LYVE-1 antibody has been utilized to monitor cancer cell trafficking in the lymphatic system in real time (McElroy et al. 2009). The recent identification of relatively specific peptides for lymphatic endothelium allowed analyses of LN lymphangiogenesis as well as tumor lymphangiogenesis (Laakkonen et al. 2002, 2004, 2008). Intravenously injected FITC conjugated LyP-1 peptide was observed to home to tumor-associated lymphatic vessels and tumor cells in MDAMB- 435 xenografts and some other tumors (Laakkonen et al. 2002, 2004, 2008). However, due to the poor tissue penetration of photons and high background of FITC, FITC-LyP-1 is not an ideal probe for lymphangiogenesis imaging in vivo.

After conjugation of the tumor lymphatic endothelium specific LyP-1 peptide with NIR fluorescent dye Cy5.5, we successfully visualized tumor-draining LN in vivo at different stages of tumor growth. The optical imaging revealed that tumor growth in the shoulder was associated

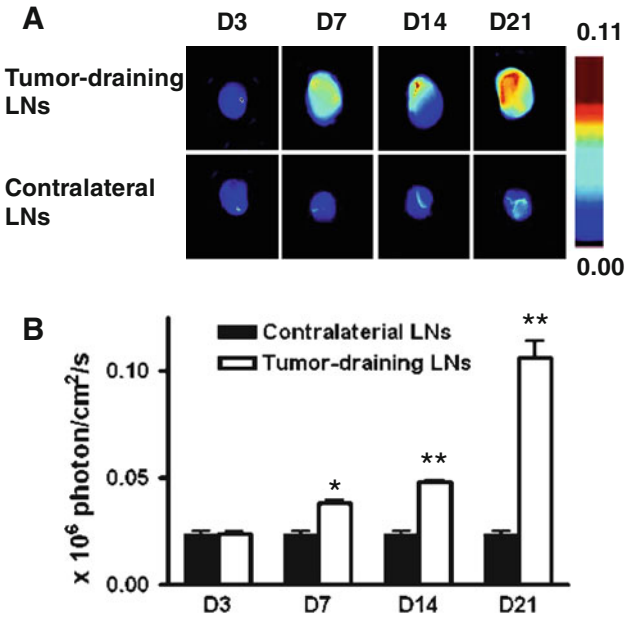

Fig. 4 Ex vivo optical imaging of lymphangiogenesis. **a** Compared with the contralateral brachial LN, the tumor-draining brachial LN was significantly enlarged at days 7, 14 and 21 after tumor cell inoculation. **b** Measurement of Cy5.5-LyP-1 fluorescence intensity in LNs. Fluorescent signal increased dramatically from day 7 to 21 in tumor-draining brachial LN (*$P < 0.05$, **$P < 0.001$)

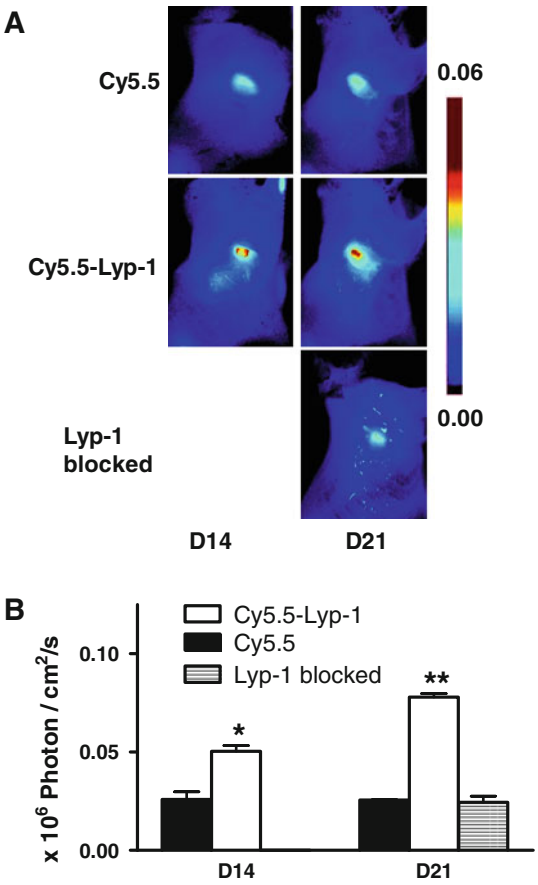

Fig. 5 **a** Optical imaging of tumor-induced lymphangiogenesis with Cy5.5-LyP-1 and Cy5.5. At days 14 and 21 after 4T1 cell inoculation, tumor-bearing BALB/C mice ($n = 3$/group), under isoflurane anesthesia, were injected with either Cy5.5-LyP-1 or Cy5.5 via the middle phalanges of both upper extremities. At 24 h post injection, the mice were killed and a dorsal skin flap was elevated to expose the tumor-draining brachial lymph nodes for fluorescence imaging. **b** Measurement of fluorescence intensity in LNs (*$P < 0.05$, **$P < 0.01$)

with increased lymphangiogenesis in the brachial LN. From day 7 to 21, the size of tumor-draining LNs did not change dramatically, while the fluorescent intensity kept increasing, indicating that the lymphatic vessel density increased along with time. This was confirmed by immunostaining with anti-LYVE-1 antibody (Fig. 6). Moreover, at 24 h after Cy5.5-LyP-1 injection, we could still identify much stronger fluorescent signals inside tumor-draining LNs than Cy5.5-LyP-1 blocked with cold compound and Cy5.5 dye only, confirming specific detection of lymphangiogenesis with this peptide probe. The results demonstrated that targeted binding of Cy5.5-LyP-1 facilitated visualization of the expansion of lymphatic network within the tumor-draining sentinel LNs, even before tumor metastasis occurred.

We also noticed that the fluorescent signal did not homogeneously distribute within the tumor-draining LNs at all stages. We speculated that this phenomenon resulted from the unique structure and pattern of lymph flow in the LNs. Within a LN, each afferent lymphatic collects lymph from a different drainage field, and each lobule is potentially exposed to different concentrations of cytokines and stimulators. Thus, lobules within the same LN may have different levels of immunological activity, and the cortical, paracortical and medullary compartments composed of these lobules will not necessarily have a uniform appearance (Sainte-Marie et al. 1982; Willard-Mack 2006). In this study, variation in the stimulation received from 4T1 tumor was likely the reason that the lymphangiogenesis within the tumor-draining LNs varied in different lobules, as reflected by both optical imaging and fluorescent immunostaining.

Conclusion

In summary, we successfully visualized lymphangiogenesis in tumor-draining LNs, along with tumor growth, using Cy5.5-labeled LyP-1 peptide. This new technology offers unique advantages over current technologies for in vivo prediction and detection of LN metastasis. It enables a strategy of demonstrating "high risk" LNs before tumor metastasis or after micro-metastasis occurs. It should be useful in both development of anti-lymphatic therapeutics and advancement of our understanding of the interactions between primary tumors and tumor-draining LNs.

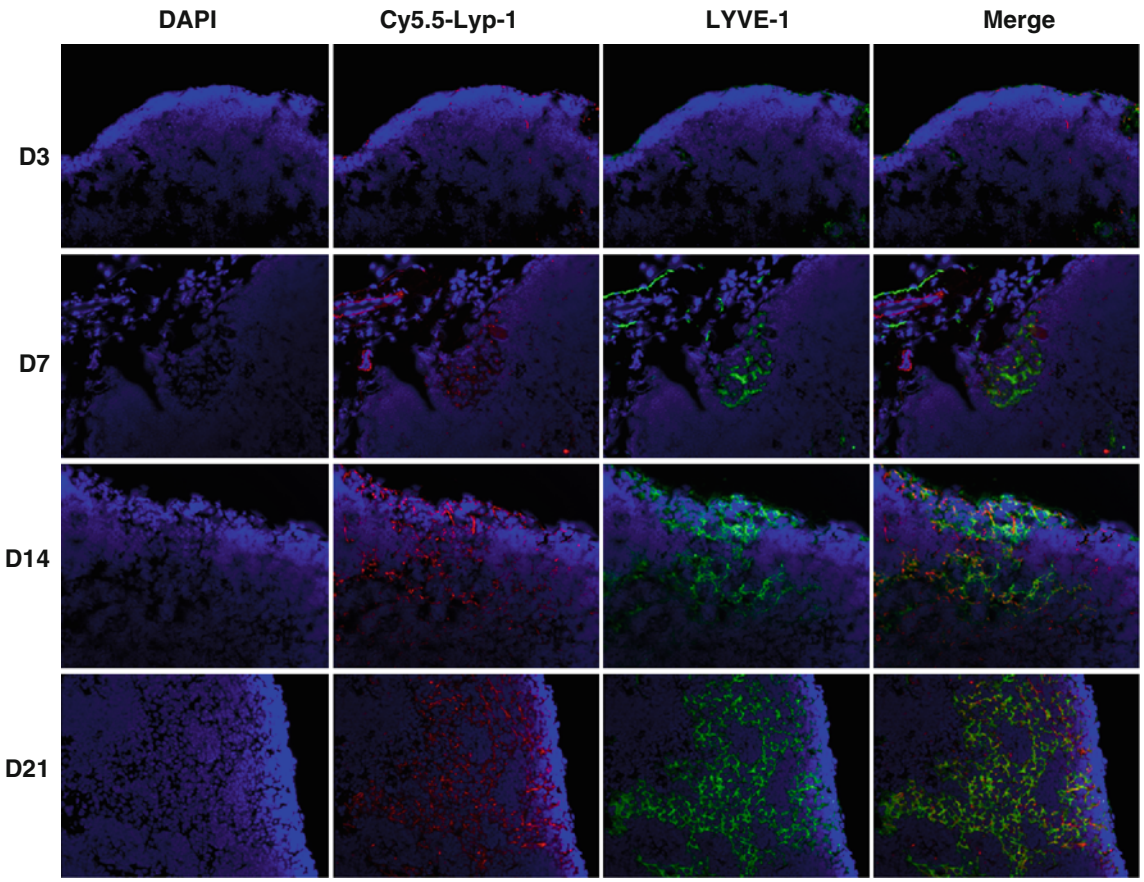

Fig. 6 Ex vivo fluorescence staining of lymph node. At 24 h after Cy5.5-LyP-1 injection, brachial lymph nodes from both sides were removed and sectioned into 4 μm slices and observed with an Olympus IX81 fluorescence microscopy. The same lymph node sections were also stained against LYVE-1, one of the most specific and widely used lymphatic endothelial markers. Nuclei were stained with DAPI

Acknowledgments This project was supported in part by the Intramural Research Program of the National Institute of Biomedical Imaging and Bioengineering (NIBIB), National Institutes of Health (NIH), the International Cooperative Program of the National Science Foundation of China (NSFC) (81028009). F.Z and G.L. are partially supported by the NSFC grant No. 30930028. G.N. currently is an Imaging Sciences Training Program (ISTP) Fellow jointly supported by the Radiology and Imaging Sciences Department, NIH Clinical Center and the Intramural Research Program, NIBIB, NIH.

References

Aslakson CJ, Miller FR (1992) Selective events in the metastatic process defined by analysis of the sequential dissemination of subpopulations of a mouse mammary tumor. Cancer Res 52(6):1399–1405

Ballou B, Ernst LA, Andreko S, Harper T, Fitzpatrick JA, Waggoner AS, Bruchez MP (2007) Sentinel lymph node imaging using quantum dots in mouse tumor models. Bioconjug Chem 18(2):389–396

Banerji S, Ni J, Wang SX, Clasper S, Su J, Tammi R, Jones M, Jackson DG (1999) Lyve-1, a new homologue of the cd44 glycoprotein, is a lymph-specific receptor for hyaluronan. J Cell Biol 144(4):789–801

Eiber M, Beer AJ, Holzapfel K, Tauber R, Ganter C, Weirich G, Krause BJ, Rummeny EJ, Gaa J (2010) Preliminary results for characterization of pelvic lymph nodes in patients with prostate cancer by diffusion-weighted mr-imaging. Invest Radiol 45(1):15–23

Harrell MI, Iritani BM, Ruddell A (2007) Tumor-induced sentinel lymph node lymphangiogenesis and increased lymph flow precede melanoma metastasis. Am J Pathol 170(2):774–786

Hirakawa S, Kodama S, Kunstfeld R, Kajiya K, Brown LF, Detmar M (2005) Vegf-a induces tumor and sentinel lymph node lymphangiogenesis and promotes lymphatic metastasis. J Exp Med 201(7):1089–1099

Hirakawa S, Brown LF, Kodama S, Paavonen K, Alitalo K, Detmar M (2007) Vegf-c-induced lymphangiogenesis in sentinel lymph nodes promotes tumor metastasis to distant sites. Blood 109(3):1010–1017

Hirakawa S, Detmar M, Kerjaschki D, Nagamatsu S, Matsuo K, Tanemura A, Kamata N, Higashikawa K, Okazaki H, Kameda K, Nishida-Fukuda H, Mori H, Hanakawa Y, Sayama K, Shirakata Y, Tohyama M, Tokumaru S, Katayama I, Hashimoto K (2009) Nodal lymphangiogenesis and metastasis: Role of tumor-induced lymphatic vessel activation in extramammary paget's disease. Am J Pathol 175(5):2235–2248

Ishii H, Chikamatsu K, Sakakura K, Miyata M, Furuya N, Masuyama K (2010) Primary tumor induces sentinel lymph node

lymphangiogenesis in oral squamous cell carcinoma. Oral Oncol 46(5):373–378

Jaffer FA, Weissleder R (2005) Molecular imaging in the clinical arena. JAMA 293(7):855–862

Ji RC (2006) Lymphatic endothelial cells, tumor lymphangiogenesis and metastasis: new insights into intratumoral and peritumoral lymphatics. Cancer Metastasis Rev 25(4):677–694

Ji RC (2009) Lymph node lymphangiogenesis: a new concept for modulating tumor metastasis and inflammatory process. Histol Histopathol 24(3):377–384

Kosaka N, Ogawa M, Sato N, Choyke PL, Kobayashi H (2009) In vivo real-time, multicolor, quantum dot lymphatic imaging. J Invest Dermatol 129(12):2818–2822

Laakkonen P, Porkka K, Hoffman JA, Ruoslahti E (2002) A tumor-homing peptide with a targeting specificity related to lymphatic vessels. Nat Med 8(7):751–755

Laakkonen P, Akerman ME, Biliran H, Yang M, Ferrer F, Karpanen T, Hoffman RM, Ruoslahti E (2004) Antitumor activity of a homing peptide that targets tumor lymphatics and tumor cells. Proc Natl Acad Sci USA 101(25):9381–9386

Laakkonen P, Zhang L, Ruoslahti E (2008) Peptide targeting of tumor lymph vessels. Ann N Y Acad Sci 1131:37–43

Licha K, Debus N, Emig-Vollmer S, Hofmann B, Hasbach M, Stibenz D, Sydow S, Schirner M, Ebert B, Petzelt D, Buhrer C, Semmler W, Tauber R (2005) Optical molecular imaging of lymph nodes using a targeted vascular contrast agent. J Biomed Opt 10(4): 41205

Mandriota SJ, Jussila L, Jeltsch M, Compagni A, Baetens D, Prevo R, Banerji S, Huarte J, Montesano R, Jackson DG, Orci L, Alitalo K, Christofori G, Pepper MS (2001) Vascular endothelial growth factor-c-mediated lymphangiogenesis promotes tumour metastasis. EMBO J 20(4):672–682

McElroy M, Hayashi K, Garmy-Susini B, Kaushal S, Varner JA, Moossa AR, Hoffman RM, Bouvet M (2009) Fluorescent lyve-1 antibody to image dynamically lymphatic trafficking of cancer cells in vivo. J Surg Res 151(1):68–73

Mumprecht V, Honer M, Vigl B, Proulx ST, Trachsel E, Kaspar M, Banziger-Tobler NE, Schibli R, Neri D, Detmar M (2010) In vivo imaging of inflammation- and tumor-induced lymph node lymphangiogenesis by immuno-positron emission tomography. Cancer Res 70(21):8842–8851. doi:10.1158/0008-5472

Qian CN, Berghuis B, Tsarfaty G, Bruch M, Kort EJ, Ditlev J, Tsarfaty I, Hudson E, Jackson DG, Petillo D, Chen J, Resau JH, Teh BT (2006) Preparing the "Soil": the primary tumor induces vasculature reorganization in the sentinel lymph node before the arrival of metastatic cancer cells. Cancer Res 66(21):10365–10376

Sainte-Marie G, Peng FS, Belisle C (1982) Overall architecture and pattern of lymph flow in the rat lymph node. Am J Anat 164(4):275–309

Schirrmeister H, Kotzerke J, Vogl F, Buck A, Czech N, Koretz K, Helm G, Kreienberg R, Kuhn T (2004) Prospective evaluation of factors influencing success rates of sentinel node biopsy in 814 breast cancer patients. Cancer Biother Radiopharm 19(6):784–790

Sharma R, Wendt JA, Rasmussen JC, Adams KE, Marshall MV, Sevick-Muraca EM (2008) New horizons for imaging lymphatic function. Ann N Y Acad Sci 1131:13–36

Stacker SA, Caesar C, Baldwin ME, Thornton GE, Williams RA, Prevo R, Jackson DG, Nishikawa S, Kubo H, Achen MG (2001) Vegf-d promotes the metastatic spread of tumor cells via the lymphatics. Nat Med 7(2):186–191

Suzuki M, Unno N, Yamamoto N, Nishiyama M, Sagara D, Tanaka H, Mano Y, Konno H (2009) Impaired lymphatic function recovered after great saphenous vein stripping in patients with varicose vein: venodynamic and lymphodynamic results. J Vasc Surg 50(5):1085–1091

Tammela T, Alitalo K (2010) Lymphangiogenesis: molecular mechanisms and future promise. Cell 140(4):460–476

Tao K, Fang M, Alroy J, Sahagian GG (2008) Imagable 4t1 model for the study of late stage breast cancer. BMC Cancer 8:228

Ting R, Aguilera TA, Crisp JL, Hall DJ, Eckelman WC, Vera DR, Tsien RY (2010) Fast ^{18}F labeling of a near-infrared fluorophore enables positron emission tomography and optical imaging of sentinel lymph nodes. Bioconjug Chem 21(10):1811–1819

Van den Eynden GG, Vandenberghe MK, van Dam PJ, Colpaert CG, van Dam P, Dirix LY, Vermeulen PB, Van Marck EA (2007) Increased sentinel lymph node lymphangiogenesis is associated with nonsentinel axillary lymph node involvement in breast cancer patients with a positive sentinel node. Clin Cancer Res 13(18 Pt 1):5391–5397

Willard-Mack CL (2006) Normal structure, function, and histology of lymph nodes. Toxicol Pathol 34(5):409–424

Winnard PT Jr, Pathak AP, Dhara S, Cho SY, Raman V, Pomper MG (2008) Molecular imaging of metastatic potential. J Nucl Med 49(Suppl 2):96S–112S